The 58-month BAT AGN catalogue: results from the Northern Galactic Cap

Ranjan Vasudevan (IoA, Cambridge),
Niel Brandt (Penn State, USA), Richard Mushotzky, Marcio Melendez, Taro Shimizu (UMD, USA), Andy Fabian (IoA, Cambridge), Poshak Gandhi (Durham)
Lisa Winter (AER, USA), Wayne Baumgartner (NASA/GSFC, USA),
Poster: Luigi Gallo (St. Mary's, Canada), Dom Walton (Caltech), Abdu Zoghbi (UMD), Anne Lohfink (Cambridge)

Vasudevan et al. (2013a) ApJ, 763, 111
Vasudevan et al. (2013b), ApJ Letters, 770, 37
Vasudevan et al. (2014), ApJ, 785, 30 (poster)
related:
Vasudevan et al. (2013c), MNRAS, 431, 3127

Swift/BAT's utility: 'unbiased' detection of AGN

- Gilli, Comastri & Hasinger (2007)

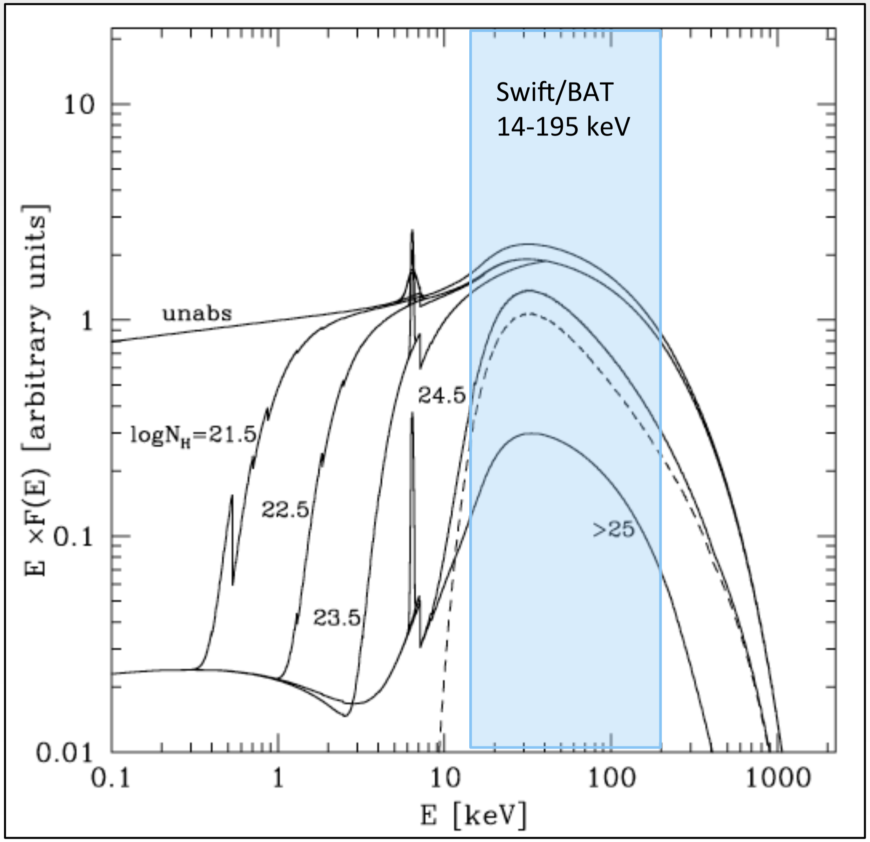

The BAT catalogue (9-month)

- Tueller et al. (2008)

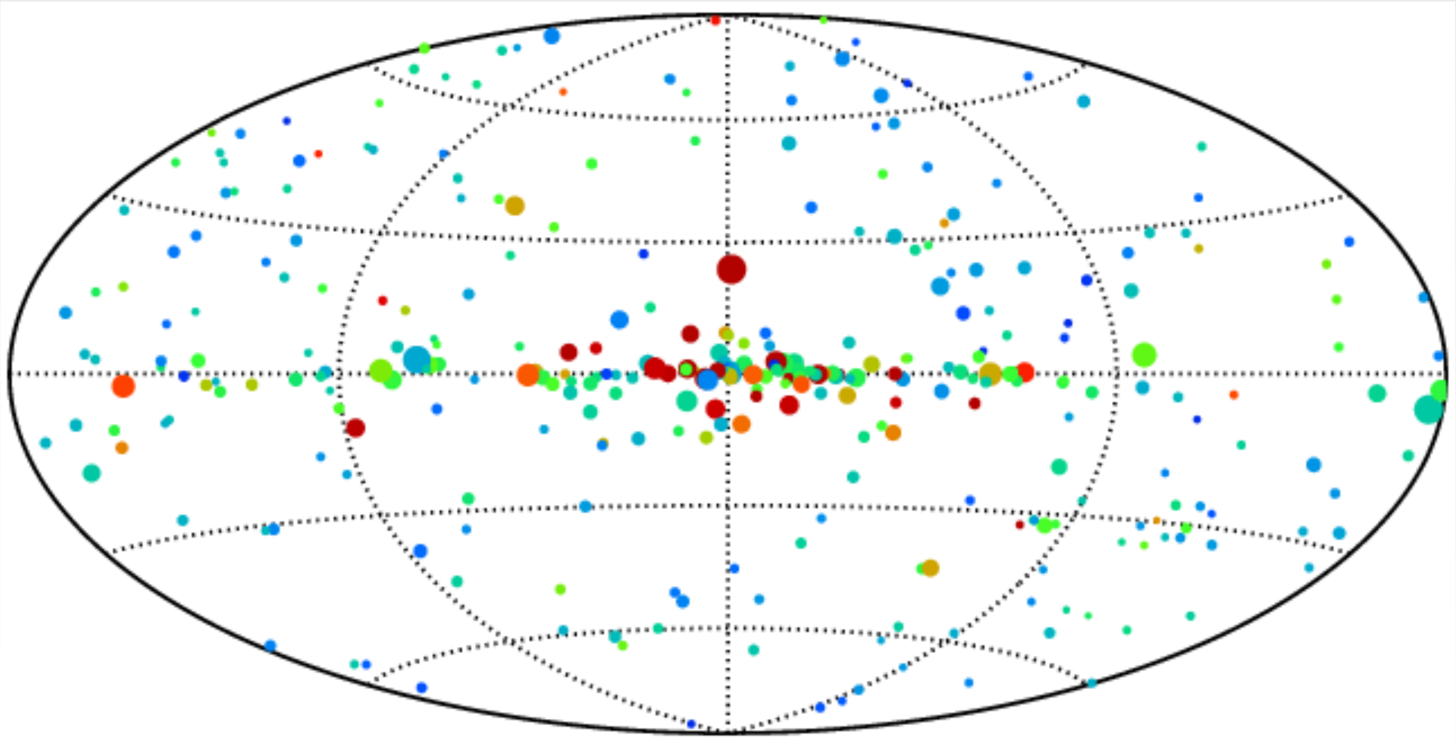

The BAT catalogue (22-month)

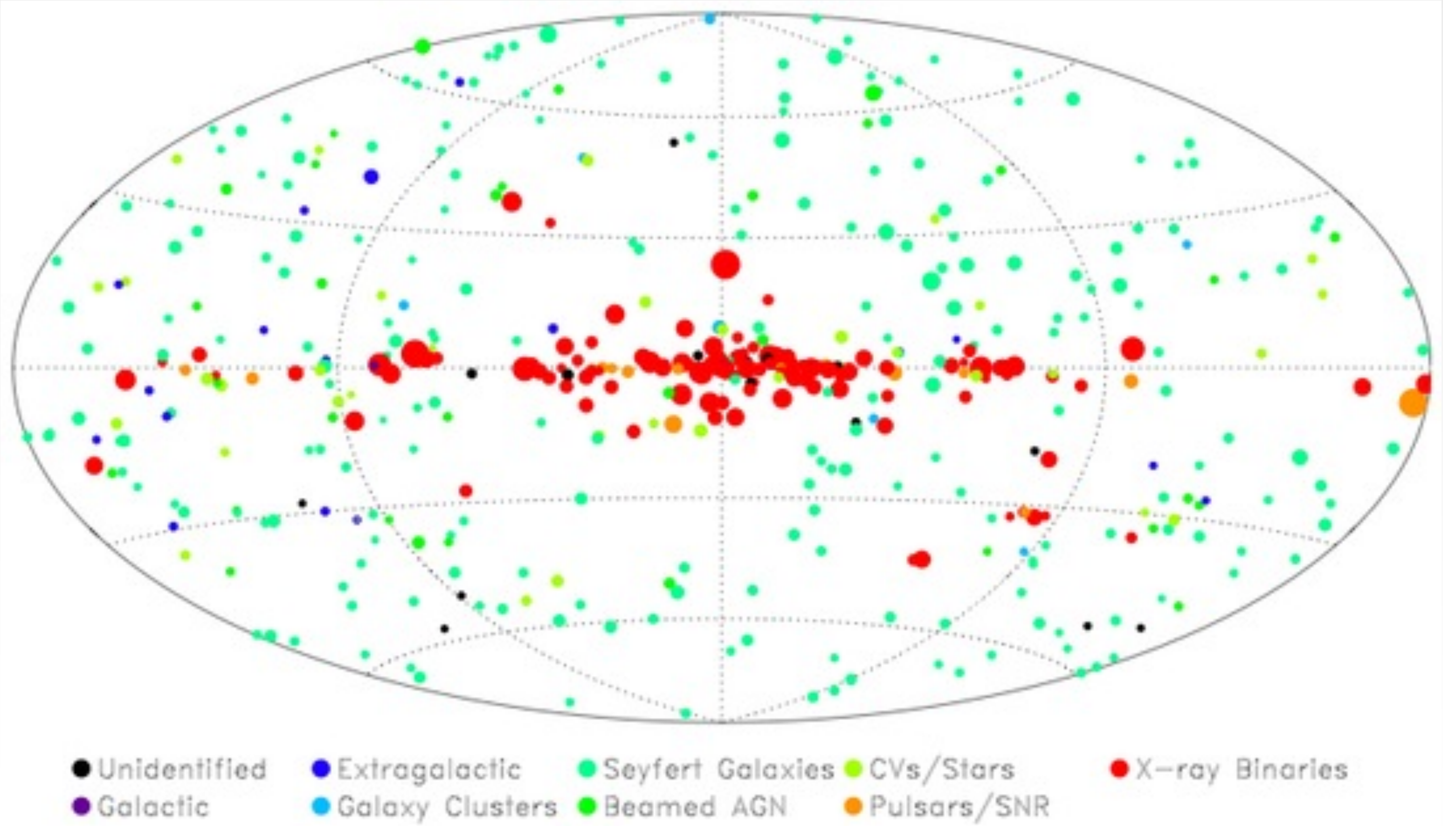

The BAT catalogue (58-month)

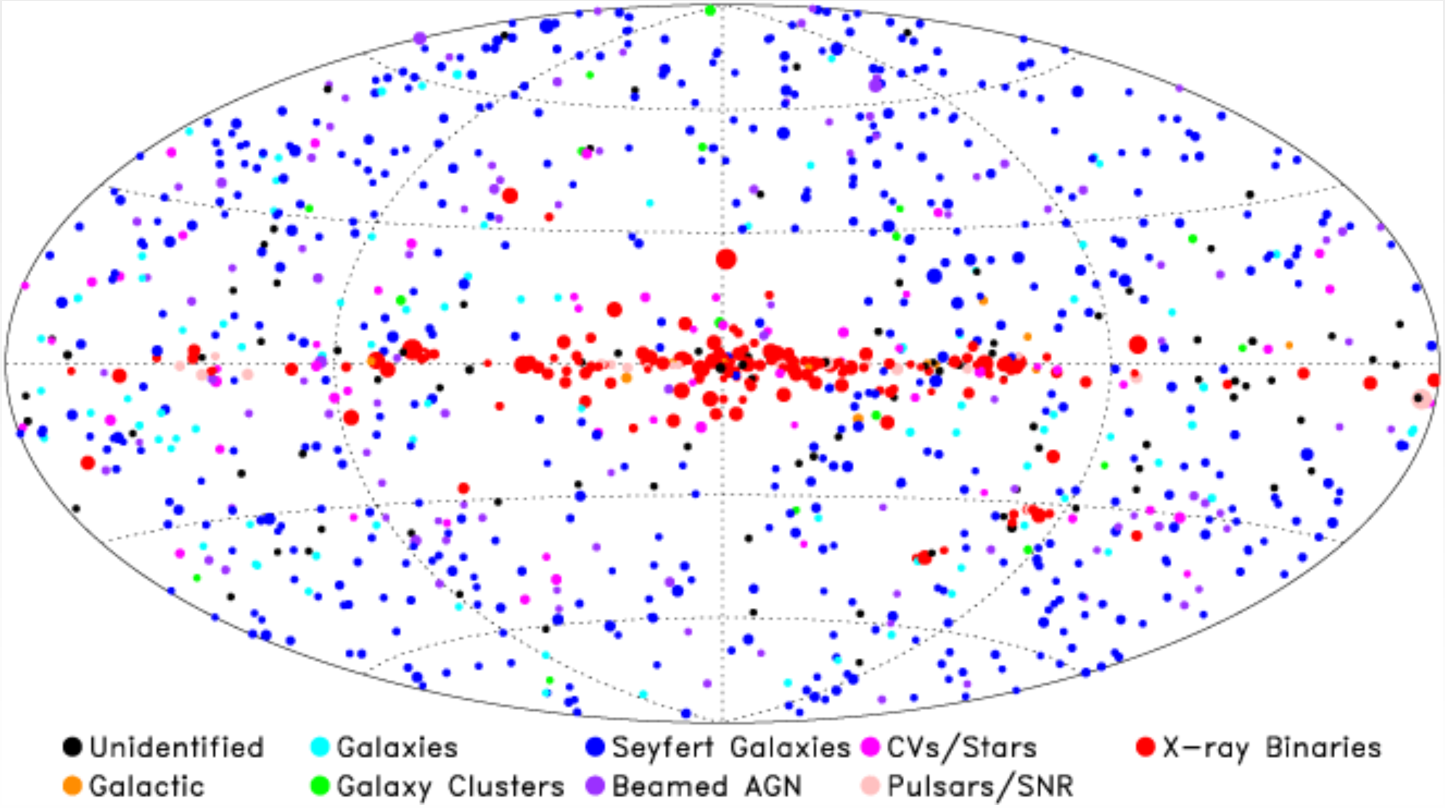

The BAT catalogue (70-month)

- Baumgartner et al. (2013)

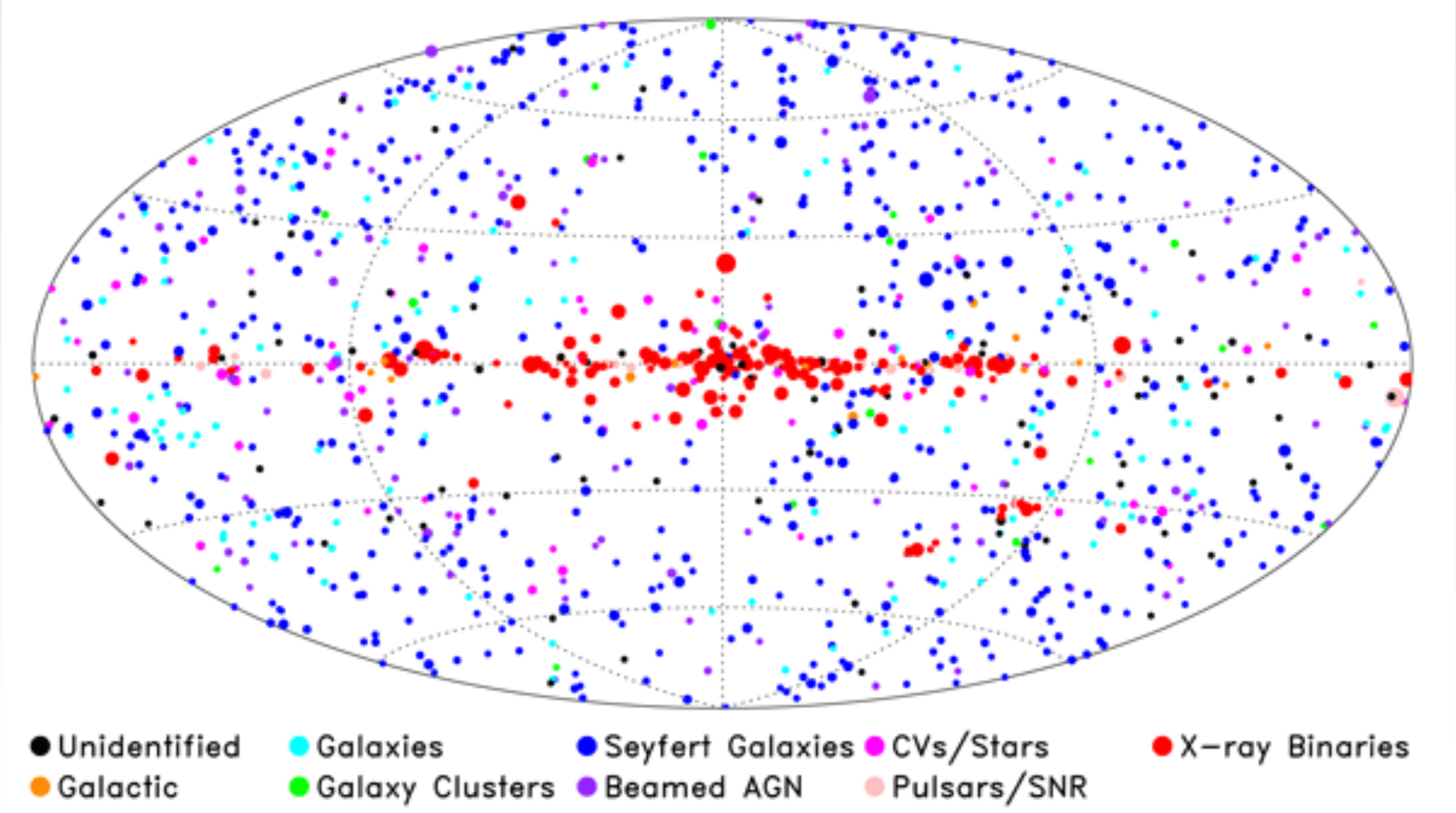

Earlier work on BAT AGN catalogue

- Winter et al. (2009, 2010, 2012) - X-ray, optical properties, outflows
- Vasudevan et al. (2009, 2010) - X-ray, optical/UV, IR, energy budget
- Burlon et al. (2011, 2013) – X-ray properties, radio properites/jets
- Matsuka et al. (2012), Melendez et al. (2014 – submitted) – hard X-ray & IR correlations, torus properties
- Ajello et al. (2008, 2012) – X-ray properties, stats
- Koss et al. (2010, 2011) – host galaxy properties of BAT AGN, merging/ clustering

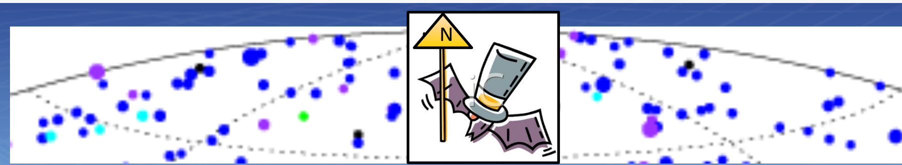

Scope

- **NB: 58-month catalogue has 720 AGN candidates** (BAT SNR > 4.8), many without XMM or equivalent coverage; Galactic plane has many local contaminants (X-ray binaries, Galactic absorption etc), so *better* ***to target a complete subsample of manageable size.***

- Therefore restrict to Galactic latitude **b > 50°** (Brandt et al. 2008 XMM proposal)**.** ***Low Galactic N_H allows analysis of soft features too***

- Performed a comprehensive analysis of a **complete subsample from the 58-month BAT catalogue** and updated the analysis of previous versions of the catalogue (Winter et al. 2009, Burlon et al. 2011)

- Determined up-to-date **absorbing column density distribution**, **luminosity distribution and details of spectral features**

- Aim: construct **multi-wavelength SEDs** for this complete sample; sky area has **complementary coverage at other wavelengths for SEDs** (e.g. SDSS, 2MASS, WISE, AKARI, GALEX+…)

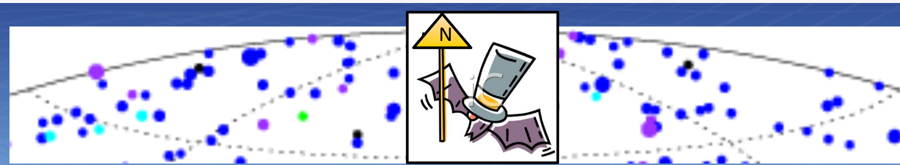

Scope

- **NB: 58-month catalogue has 720 AGN candidates** (BAT SNR > 4.8), many without XMM or equivalent coverage; Galactic plane has many local contaminants (X-ray binaries, Galactic absorption etc), so *better* ***to target a complete subsample of manageable size.***

- Therefore restrict to G dt et al. 2008 XMM proposal)**.** ***Low Galactic N_H allow*** ***oo***
- Performed a comprehe **e subsample from the 58-month BAT catalogue** previous versions of the catalogue (Winter et a
- Determined up-to-dat **distribution, luminosity distribution and detai**
- Aim: construct **multi-wavelength SEDs** for this complete sample; sky area has **complementary coverage at other wavelengths for SEDs** (e.g. SDSS, 2MASS, WISE, AKARI, GALEX+…)

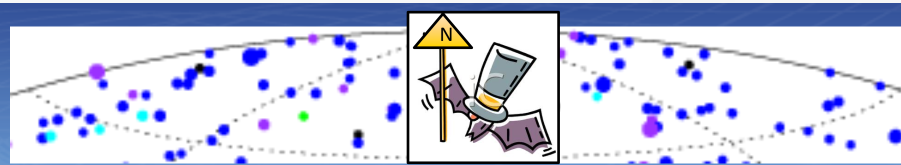

Sample properties: key statistics

- **106 non-blazar AGN candidates** (at SNR > 4.8)
- **High proportion have** targetted **XMM** data (49 objects)
- Targetted **Swift/XRT** observations for 46 objects
- **ASCA/Tartarus** archival objects used for 6 objects
- 5 objects without data at the time of writing
- Local: $z < 0.2$

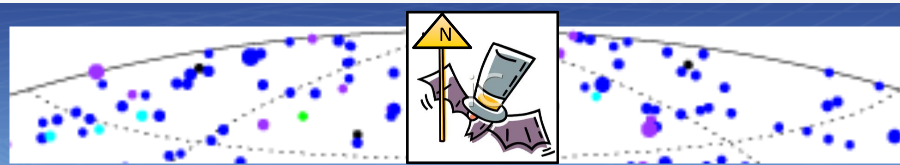

Analysis: spectral fitting

Model Combinations Used

Model Identifier	XSPEC Model String	Description
Simple power-law models		
S1	TBABS(POWERLAW)	Power-law with Galactic absorption only
S2	TBABS(ZTBABS(POWERLAW))	Absorbed power-law with Galactic and intrinsic (neutral) absorption
S3	TBABS(ZTBABS(POWERLAW+ZGAUSS))	As for S2, with a Fe Kα line at (default) 6.4 keV
S4	TBABS(ZTBABS(POWERLAW+ZBBODY))	As for S2, with a soft excess modeled as a blackbody
S5	TBABS(ZTBABS(ZEDGE(POWERLAW)))	As for S2, with an edge at 0.73 keV (default) to model a warm absorber
S6	TBABS(ZTBABS((POWERLAW+ZBBODY+ZGAUSS)))	As for S2, with both a soft excess and Fe Kα line
S7	TBABS(ZTBABS(ZEDGE(POWERLAW+ZGAUSS)))	Absorbed power-law with warm-absorber edge and Fe Kα line
S8	TBABS(ZTBABS(ZEDGE(POWERLAW+ZGAUSS+ZBBODY)))	Absorbed power-law with warm-absorber edge, Fe Kα line and soft excess
S9	TBABS(ZTBABS(ZEDGE(ZEDGE(POWERLAW))))	Absorbed power-law with two warm-absorber edges at 0.73 and 0.87 keV (default energies)
S10	TBABS(ZTBABS(ZEDGE(ZEDGE(POWERLAW+ZGAUSS))))	Absorbed power-law with two warm-absorber edges and a Fe Kα line
S11	TBABS(ZTBABS(ZEDGE(ZEDGE(POWERLAW+ZGAUSS+ZBBODY))))	Absorbed power-law with two warm-absorber edges, Fe Kα line and soft excess
Complex models (partial covering)		
C1	TBABS(ZPCFABS(POWERLAW))	Partially covered absorbed power-law with Galactic absorption
C2	TBABS(ZPCFABS(POWERLAW+ZGAUSS))	As for C1, including a Fe Kα line at (default) 6.4 keV

Analysis: spectral fitting

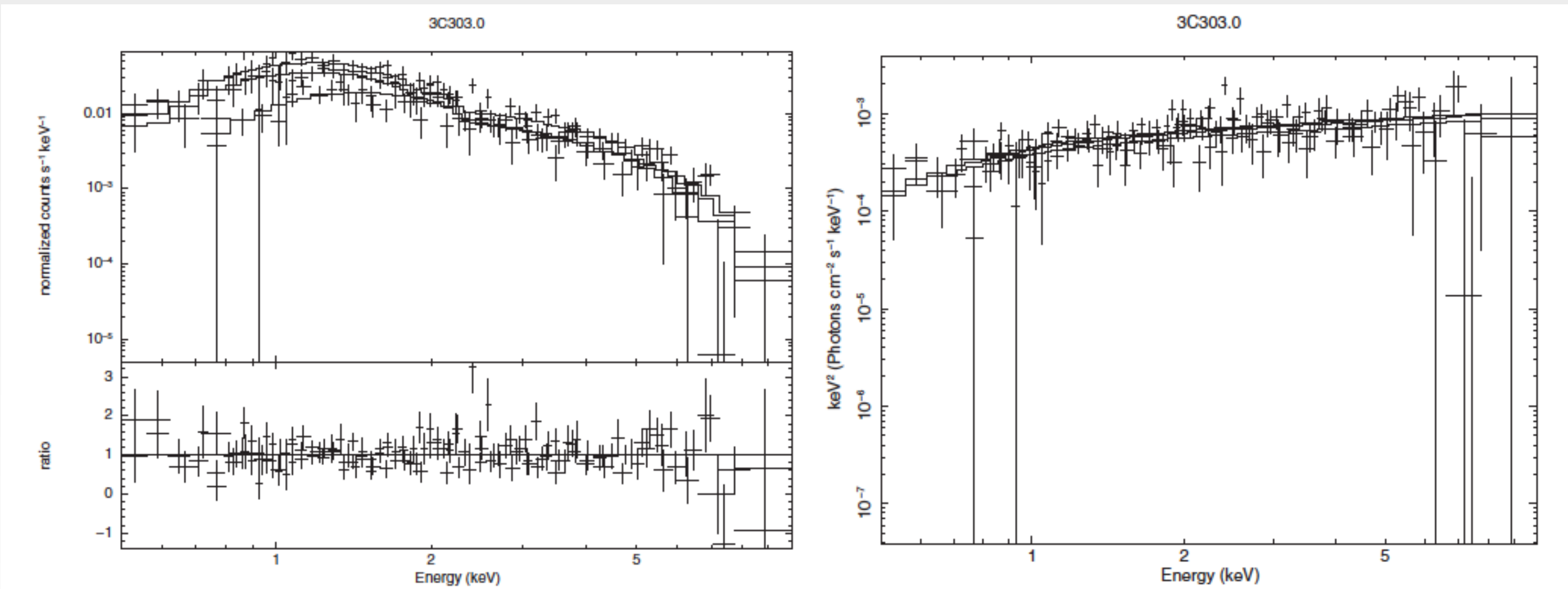

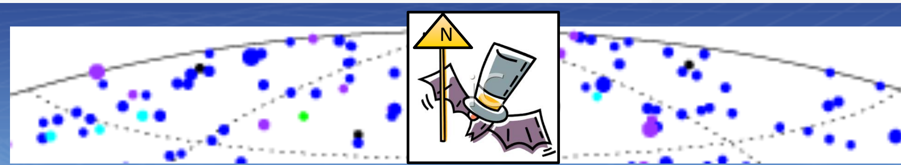

Results: column density distribution

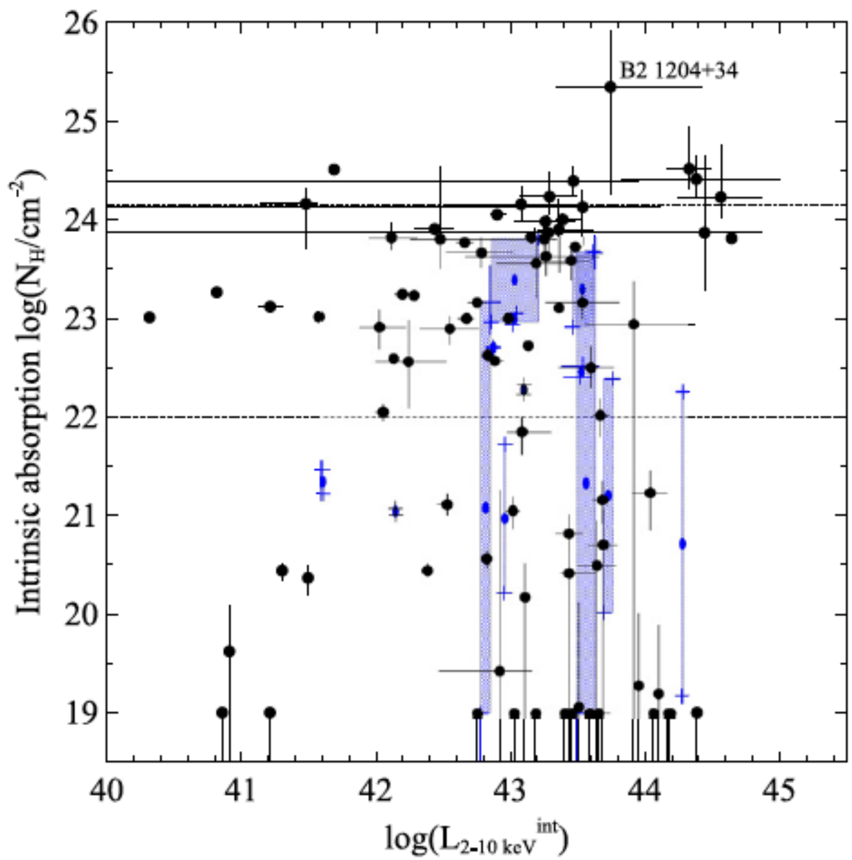

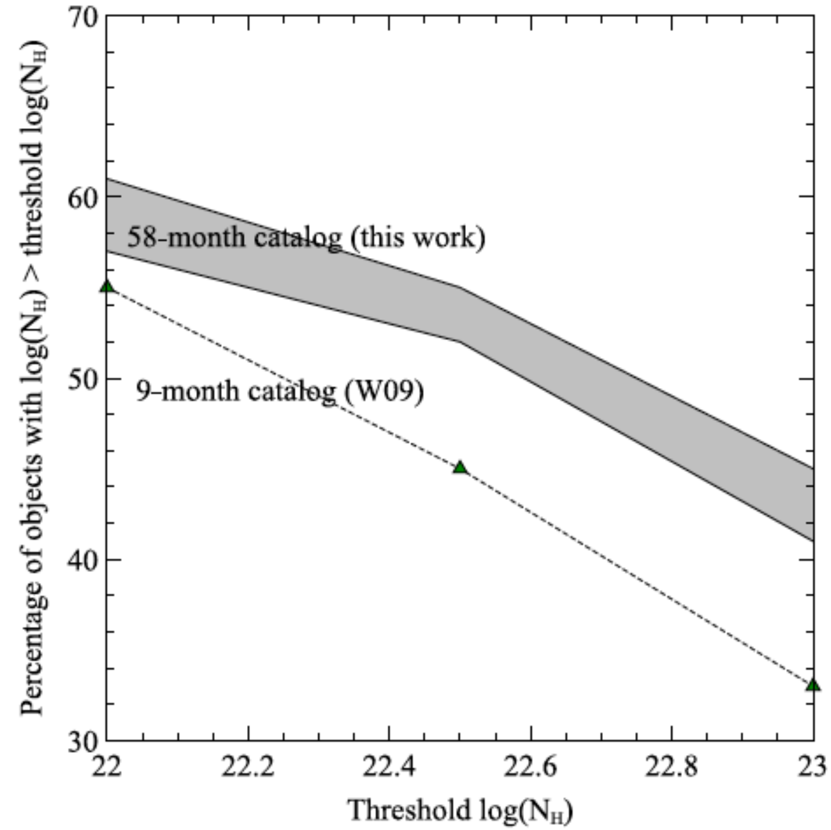

Resuts: column density distribution and flux limit

- **5 times fainter** detection limit than 9-month catalogue, uncovers wider absorption distribution

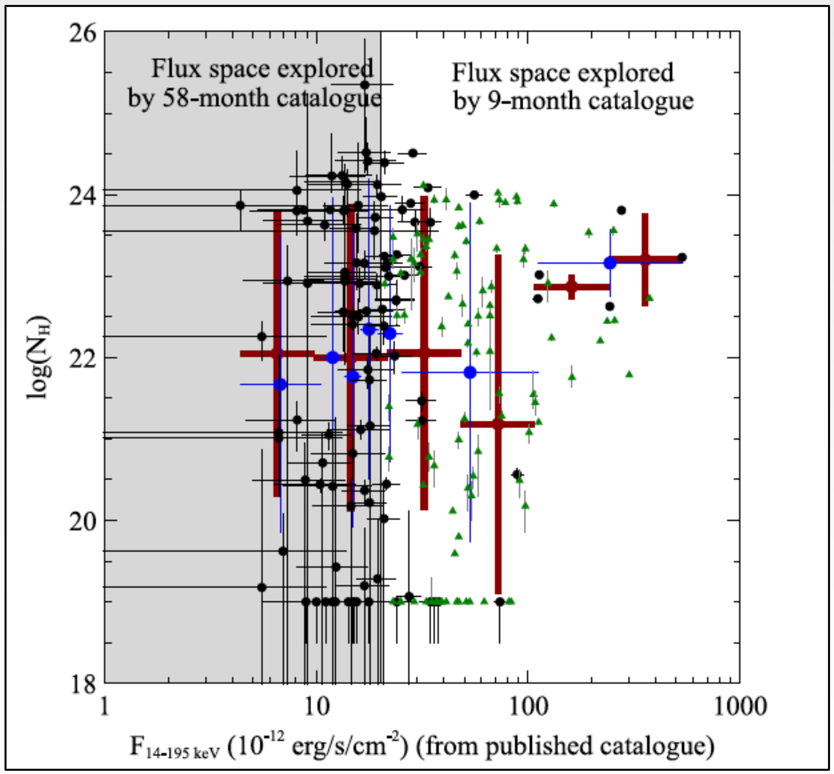

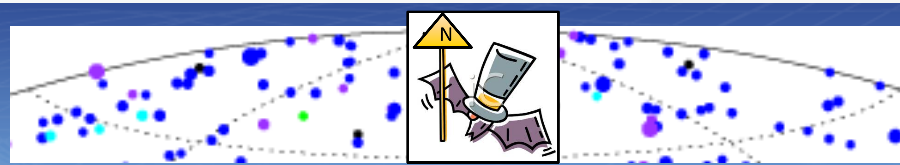

Results: column density distribution – some statistics

- **57-61 per cent** with **logNH>22**
- **41-45 per cent** with **logNH>23**
- **9 per cent Compton Thick** (logNH>24.15)
- These fractions use a **basic absorption** model (no Compton scattering – see Monday's Extragalactic Surveys talks – e.g. Georgantopoulous talk)
- More robust '**plcabs'** includes Compton scattering but degeneracies involved; **yields lower columns** by factor ~0.65 and would **reduce the Compton Thick fraction** (c.f. 4.6% from Burlon et al. 2011 for 36-month catalogue); MyTorus (Murphy & Yaqoob 2009) may yield different results

Results: luminosity distribution

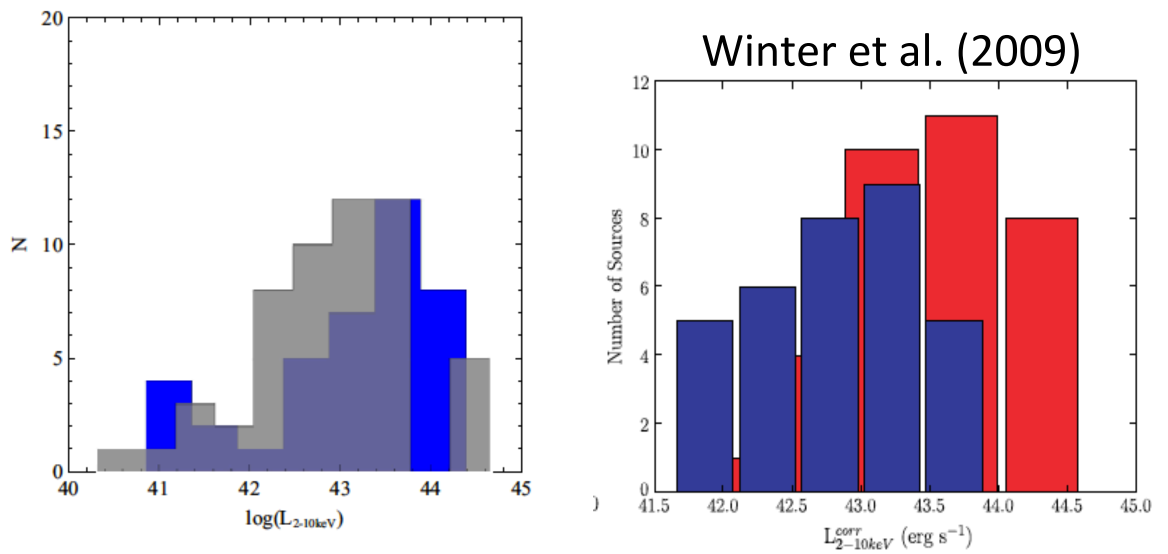

Fig. 16.— Histograms of intrinsic 2–10 keV luminosity $\log(L_{2-10\mathrm{keV}})$. The grey shaded portions represent high-absorption objects ($\log(N_H) > 22$), whereas the blue shaded portions represent low-absorption objects ($\log(N_H) < 22$).

Results: spectral features

Table 7
Comparing BAT Catalogs: Luminosity and Prevalence of X-Ray Features

Catalog (1)	$\langle \log L_{2-10\,\mathrm{keV}} \rangle, \sigma$ (All) (2)	$\langle \log L_{2-10\,\mathrm{keV}} \rangle, \sigma$ ($\log N_H < 22$) (3)	$\langle \log L_{2-10\,\mathrm{keV}} \rangle, \sigma$ ($\log N_H > 22$) (4)	Fe Kα % (5)	Soft Excess % (6)	Hidden/Buried % (7)
9 month	43.01 (0.87)	43.42 (0.79)	42.67 (0.78)	81%	41%	24%
22 month	42.70 (0.93)	42.80–42.84 (0.90–0.95)	42.60–42.65 (0.93–0.95)	75%	32%–36%	28%
58 month	43.00 (0.91–0.92)	43.02–43.07 (0.96–0.98)	42.91–42.97 (0.89)	79%	31%–33%	13%–14%

Ionised absorber edges (OVII and OVIII): 18% (or 32% of unabsorbed logNH<22 AGN)

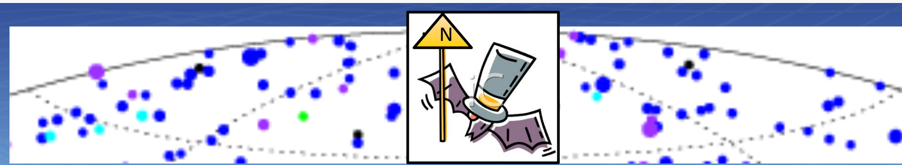

Results: Iron K-α line properties

See also papers by Ricci et al. (2013, 2014, talk earlier today) on “X-ray Baldwin/Iwasawa-Taniguchi Effect”, confirms slope of Page et al. (2004), Jiang et al. (2006), Bianchi et al. (2007)

- ▲ logNH<22
- ■ 22<logNH<23
- ● logNH>23

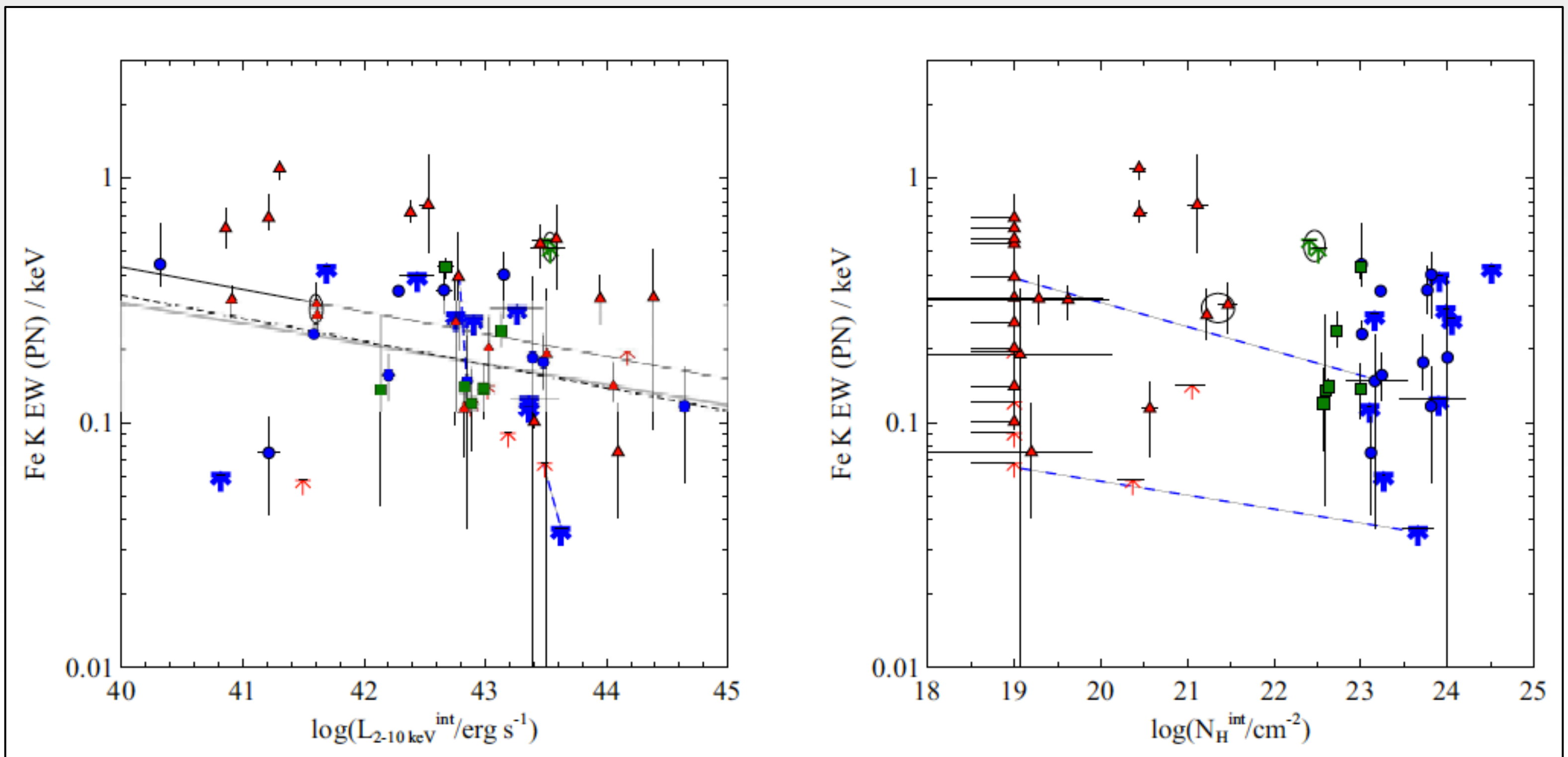

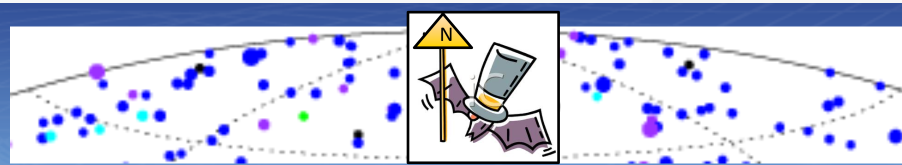

Results: soft X-ray (0.4-2keV) excess (see poster)

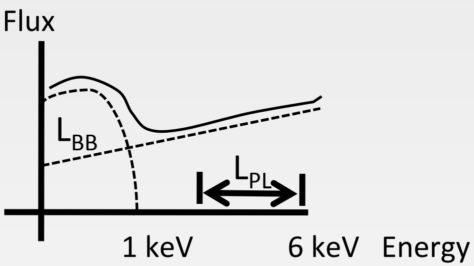

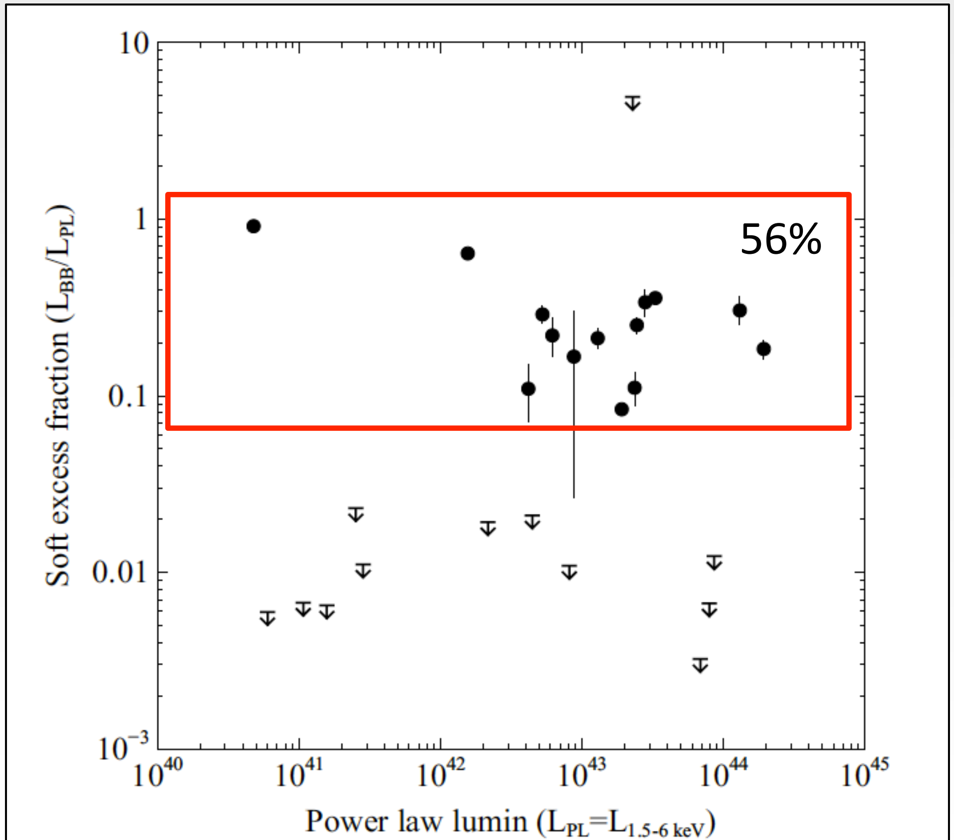

All unabsorbed (logNH<22)

Soft excess fraction = L_{BB}/L_{PL}

Results: Compton reflection

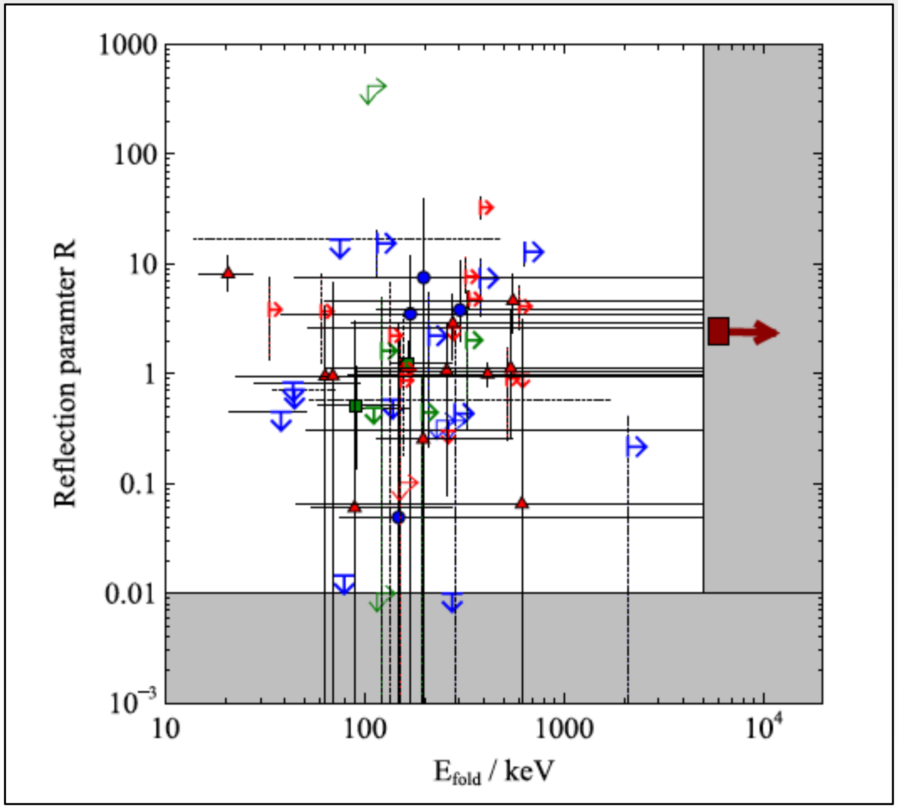

- ▲ logNH<22
- ■ 22<logNH<23
- ● logNH>23

<R>=2.7+/-0.75

Fold energy outside BAT bandpass on average

BAT renormalisation allows 3 reflection parameters to be better constrained by removing a degree of freedom

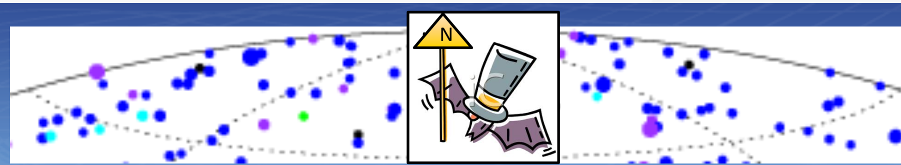

Spin-off studies: the origin of the soft excess using broad-band X-ray data

Vasudevan et al. (2014), ApJ, 785, 30

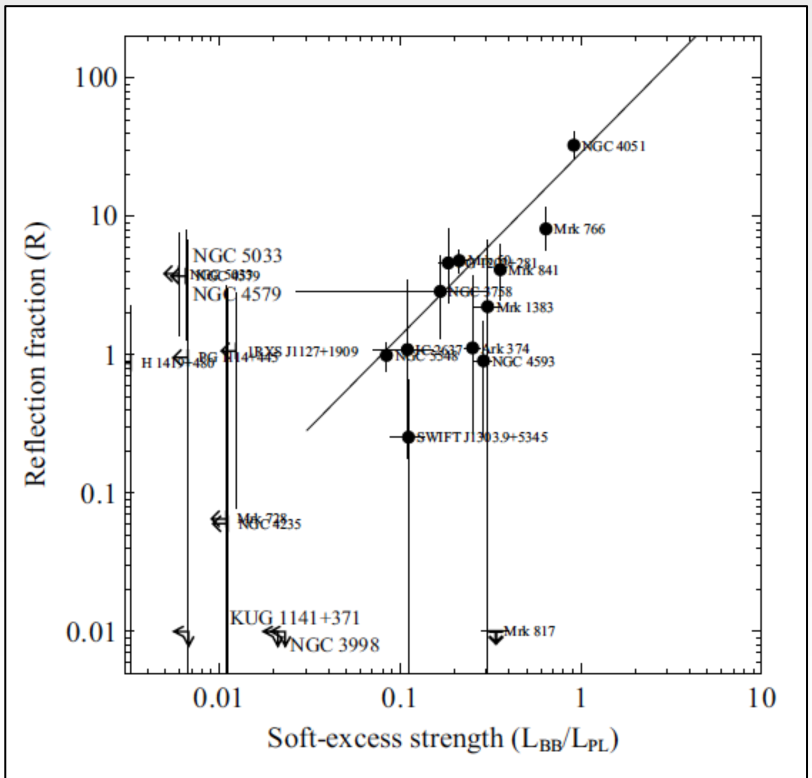

See poster I8 (I10 in programme) Also see poster F06 – Boissay et al. (paper in prep.)

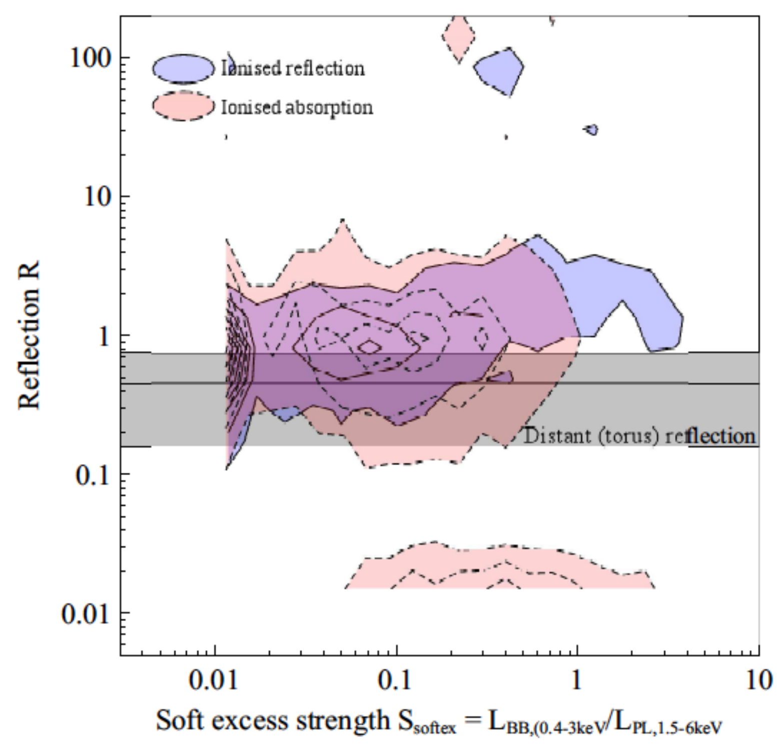

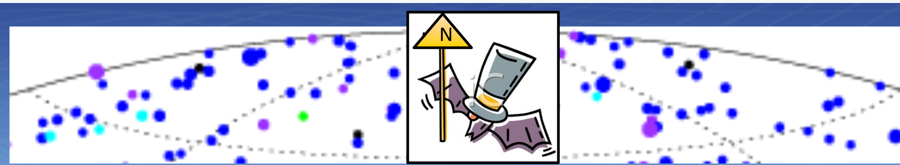

Spin-off studies: Can we reproduce the X-ray background spectrum using local AGN?

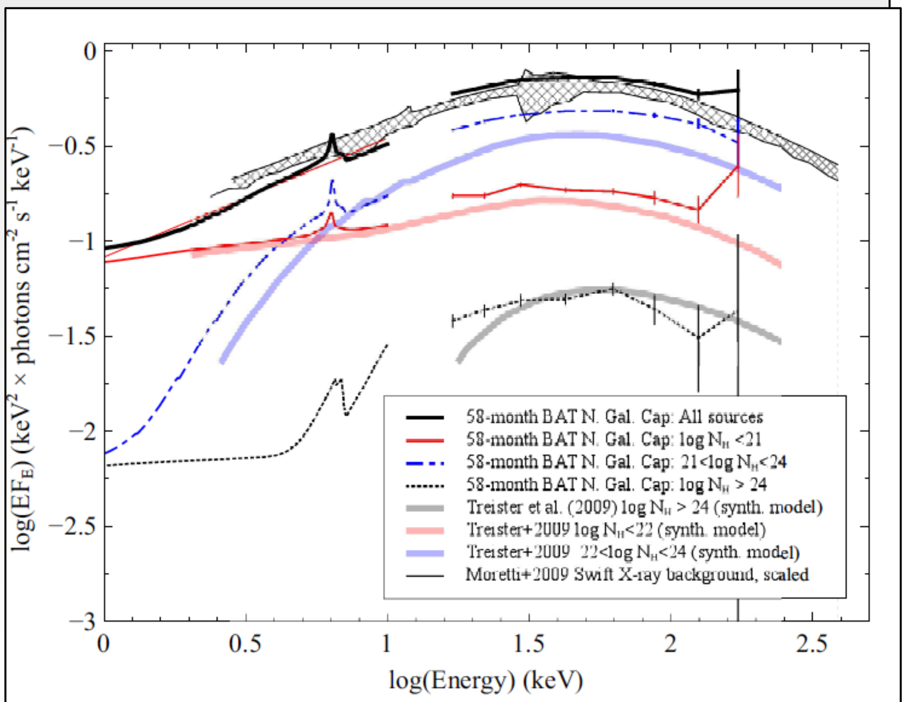

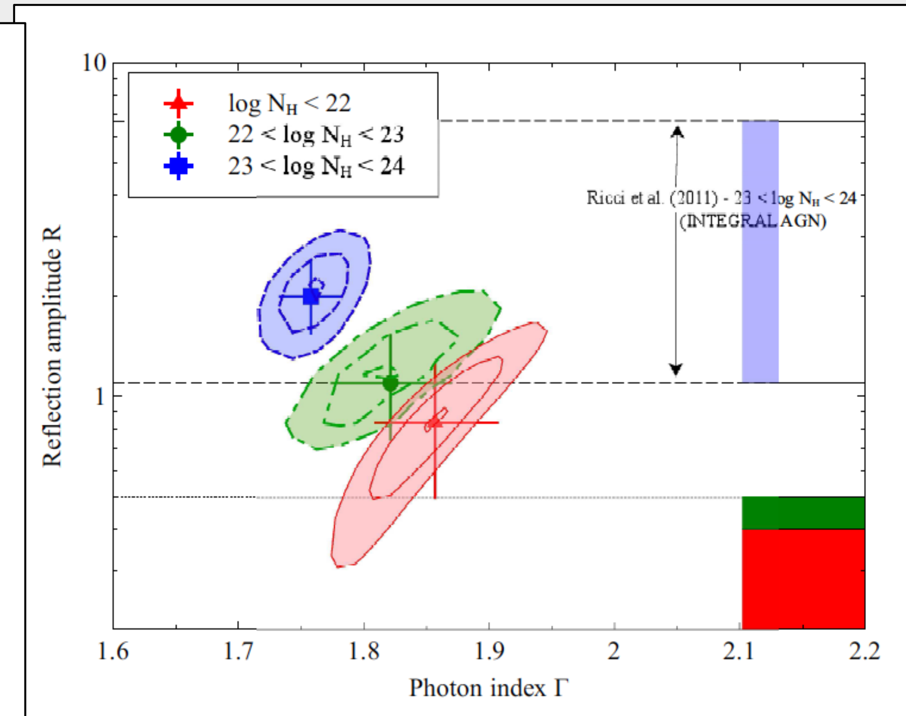

See X-ray background synthesis models of e.g. Akylas et al. (2012) – also R. Walter talk on Monday (Extragalactic Surveys & Populations, CXB session), Ricci et al. (2011)

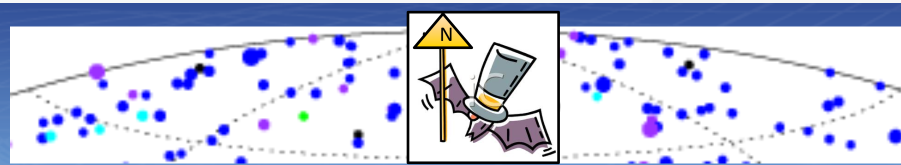

Future work: multi-wavelength AGN SEDs for a complete sample

Vasudevan et al. (2013), MNRAS, 431, 3127

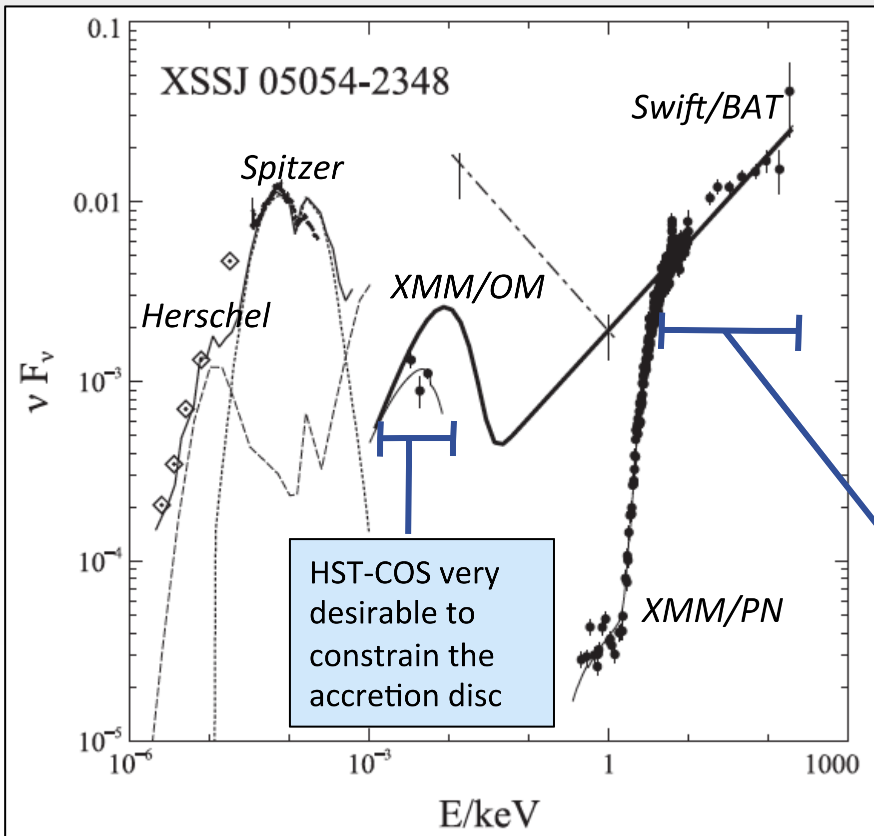

Uses:

- Bolometric luminosities/bolometric corrections (Vasudevan et al. 2007, 2009a,b, 2010)
- If good UV, accretion efficiencies – Davis & Laor (2011), Raimundo et al. (2012), Trakhtenbrot (2014), talk by Matthew Middleton (Monday)
- Relative power emitted in the corona vs. the disc
- If coupled with M_{BH} estimates, can study effect of radiation pressure (λ_{Edd}) on absorption (N_H)

NuSTAR campaign to observe ~200 BAT AGN; reflection and coronal properties constrained (Marinucci talk)

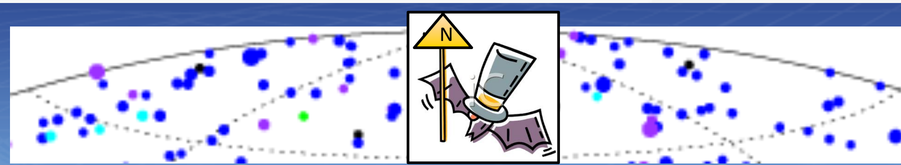

Summary

- The Northern Galactic Cap is **a complete, hard X-ray selected, representative local AGN sample**
- We have already produced key results on **the absorption and luminosity distribution, spectral features, connection to the X-ray background**
- This sampled has ‘inspired’ **simulation work on the soft excess** production mechanism (poster I8/10)
- The extensive multi-wavelength archival data is **ripe for broad-band SEDs**, which will give a complete picture of **bolometric accretion luminosity output** and shed light on other issues e.g. radiation pressure vs. absorption
- Plenty of scope for **proposals, e.g. NuSTAR, XMM, HST-COS…**

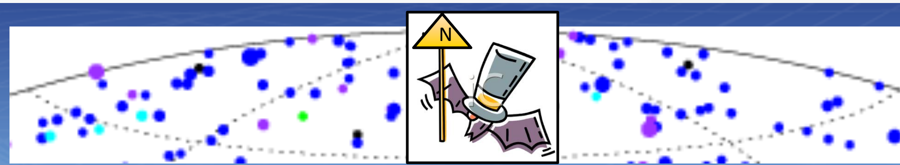

Summary

- The Northern Galactic Cap is **a complete, hard X-ray selected, representative local AGN sample**

- We have already produ **orption and luminosity distribution, spectral fe X-ray background**

- This sampled has 'inspi **e soft excess** production mechanism (poster I8/1

- The extensive multi-wa **pe for broad-band SEDs,** which will give a compl **ccretion luminosity output** and shed li pressure vs. absorption

- Plenty of scope for **T-COS…**

Vasudevan et al. (2013a) ApJ, 763, 111
Vasudevan et al. (2013b), ApJ Letters, 770, 37
Vasudevan et al. (2014), ApJ, 785, 30 (poster I8)
Vasudevan et al. (2013c), MNRAS, 431, 3127

Extra slides

Using broad-band (0.4-200 keV) data – renormalising BAT data

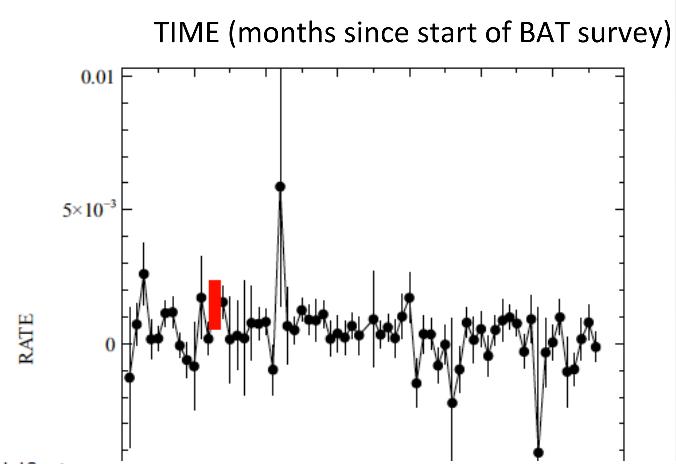

XRT + BAT fit **before** renormalisation

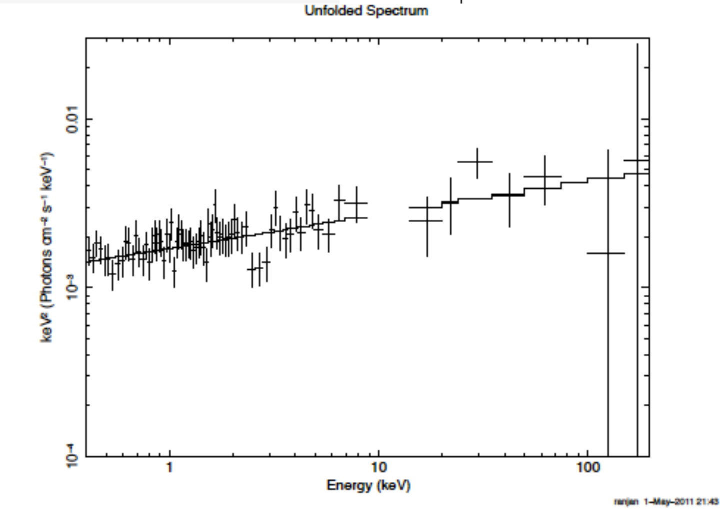

XRT + BAT fit **after** renormalisation (done for ~40% of sample)

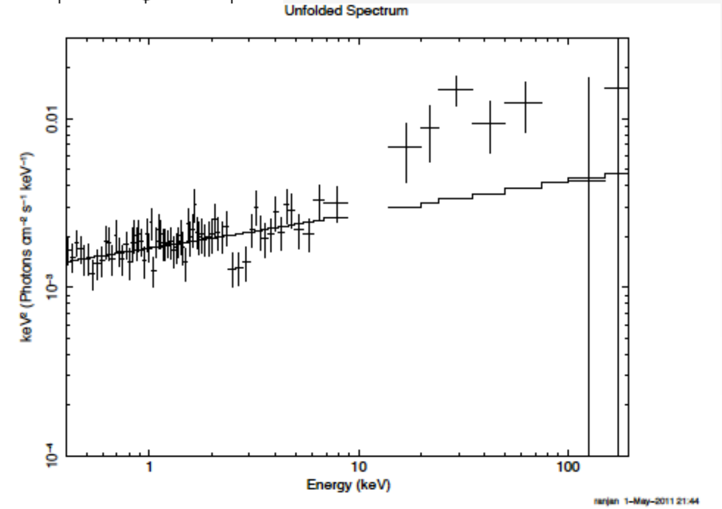

Counts distribution

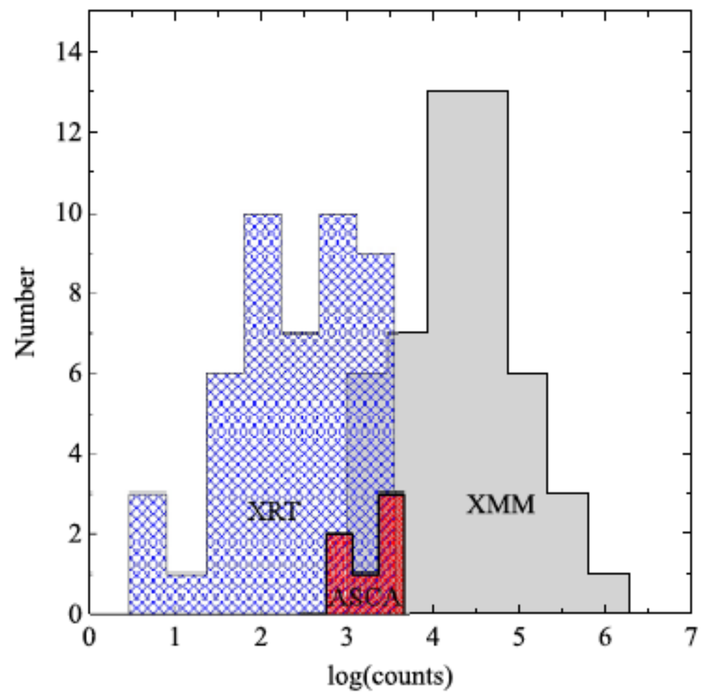

Figure 1. Histogram of total counts (0.4–10 keV) per observation for the 100 objects in our study. *XMM-Newton* (49 objects) clearly shows far superior counts statistics compared to *Swift/XRT* (46 objects) and *ASCA* (6 objects).

(A color version of this figure is available in the online journal.)

From data to results

Table 1
Table of Observations Used for Each Object

AGN	Redshift	R.A.	Decl.	l	b	Instrument	ObsID	Obs. Date	Source Counts	Obs. Time (ks)	Usable % of obs.	Optical Type	BAT Flux (SNR)
3C 234	0.1849	150.457	28.785	200.208	52.708	*XMM*	0405340101	2006-04-24	9214	39.9	84	Sy1/Sy2	8.73 (5.10)
NGC 3227	0.0039	155.878	19.865	216.992	55.446	*XMM*	0101040301	2000-11-28	53612	40.1	99	Sy1.5	112.78 (56.21)
SDSS J104326.47+110524.2	0.0476	160.860	11.089	234.761	55.932	XRT	00040954001	2010-10-29	2085	9.8	–	Sy1	14.85 (4.84)
MCG +06-24-008	0.0259	161.203	38.181	182.222	61.326	XRT	00040955004	2010-10-31	133	4.4	–	galaxy	13.69 (5.04)
UGC 05881	0.0206	161.679	25.932	208.222	62.148	XRT	00037314002	2008-07-03	217	8.8	–	Sy2	20.94 (10.42)

Table 3
Basic Fit Results

AGN	Model (χ^2/dof, P(Null Hyp.)) (1)	N_H^{Gal} (2)	N_H (Covering Fraction) (3)	Γ (4)	$F_{0.5-2\,keV}$ (5)	$F_{2-10\,keV}$ (6)	$L^{int}_{0.5-2\,keV}$ (7)	$L^{int}_{2-10\,keV}$ (8)	$L_{14-195\,keV}$ (9)	RL = $L_{5\,GHz}/L^{int}_{2-10\,keV}$ (10)
3C 234	C2 (658.26/361, 0.000)	1.76	$23.81^{+0.02}_{-0.02}$ (0.98)	$2.20_{-0.01}$	0.94	12.54	44.70	$44.64^{+0.02}_{-0.00}$	44.9 (44.6†)	<−5.331
NGC 3227	C2 (1988.13/1775, 0.000)	1.99	$23.02^{+0.01}_{-0.01}$ (0.92)	$1.50^{+0.01}$	3.83	84.25	41.18	$41.58^{+0.01}_{-0.02}$	42.6 (42.7)	−3.917
SDSS J104326.47+110524.2	S2+BAT (80.53/89, 0.728)	2.47	$20.82^{+0.19}_{-0.32}$	$1.83^{+0.10}_{-0.09}$	29.18	51.99	43.26	$43.43^{+0.10}_{-0.10}$	43.9 (43.8)	<−5.403
MCG +06-24-008	C1+BAT (4.72/7, 0.694)	1.26	$23.81^{+0.55}_{-1.26}$ ($0.79^{+0.21}_{-0.48}$)	$1.50^{+0.46}$	9.04	46.06	42.81	$43.20^{+0.90}_{-0.81}$	43.3 (43.3)	−4.895
MCG +06-24-008	S2+BAT (6.04/8, 0.643)	1.26	$22.96^{+0.31}_{-1.05}$	$1.50^{+0.38}$	0.18	34.11	42.46	$42.85^{+0.33}_{-0.47}$	43.3 (43.3)	−4.671
UGC 05881	C1+BAT (7.81/13, 0.856)	2.51	$24.39^{+0.15}_{-0.14}$ ($0.92^{+0.03}_{-0.09}$)	$2.05^{+0.15}_{-0.31}$	22.63	33.48	43.44	$43.47^{+0.48}_{-43.47}$	43.3 (43.6†)	−5.245

Table 4
Fit Results—Detailed Features (iron Kα Lines, Soft Excesses and Warm-absorber Signatures) for Objects with >4600 counts in the Fit Spectra

AGN	Model	E_{FeK} (1)	EQW$_{FeK}$ (2)	E_{softex} (3)	S_{softex} (4)	L_{BB} (5)	$\tau_{[O\,VII]}$ (6)	$E_{[O\,VII]}$ (7)	$\tau_{[O\,VIII]}$ (8)	$E_{[O\,VIII]}$ (9)
3C 234	C2	6.40*	$0.117^{+0.052}_{-0.060}$	...	...	...	...	...	...	...
NGC 3227	C2	$6.40^{+0.01}_{-0.01}$	$0.230^{+0.028}_{-0.010}$	...	...	...	...	...	...	...
Mrk 728	S3	$6.36^{+0.06}_{-6.36}$	$0.201^{+0.070}_{-0.055}$	...	<0.011	...	<0.017	...	...	...
IC 2637	S6	6.40*	$0.256^{+0.146}_{-0.158}$	$0.203^{+0.020}_{-0.026}$	$0.110^{+0.041}_{-0.039}$	$0.005^{+0.002}_{-0.002}$	<0.043	...	...	...
PG 1114+445	S10	$6.40^{+0.06}_{-0.05}$	$0.141^{+0.036}_{-0.020}$	...	<0.007	...	$2.131^{+0.139}_{-0.127}$	0.73	$0.534^{+0.100}_{-0.105}$	0.87
1RXS J1127+1909	S7	6.40*	$0.076^{+0.044}_{-0.035}$	...	<0.012	...	$0.794^{+0.071}_{-0.069}$	0.73	...	...

Radio loudness

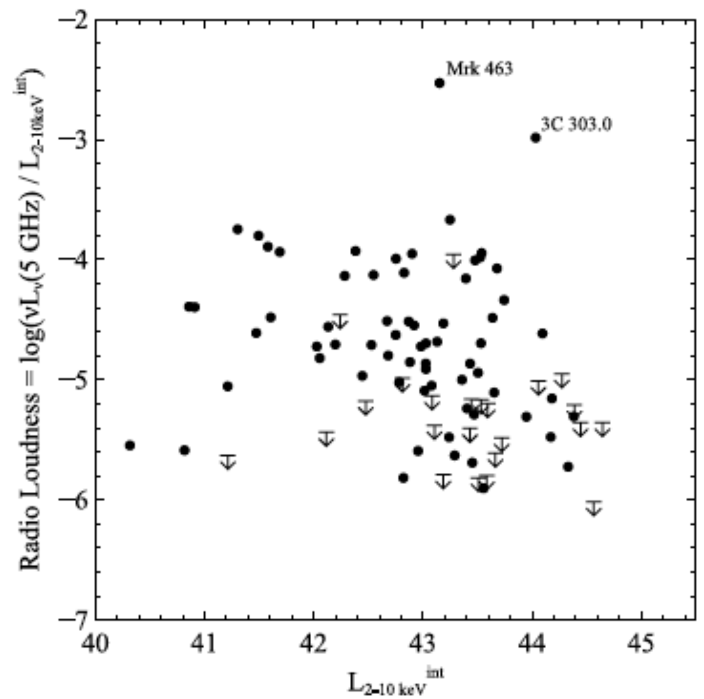

Figure 9. Radio loudness ($\nu L_\nu(\nu = 5\,\mathrm{GHz})/L_{2-10\,\mathrm{keV}}$) against intrinsic 2–10 keV luminosity. Downward-pointing arrows show upper limits where FIRST radio detections were not available (assuming a flux limit of 0.75 mJy to calculate the luminosities).

Absorbed fraction vs. luminosity

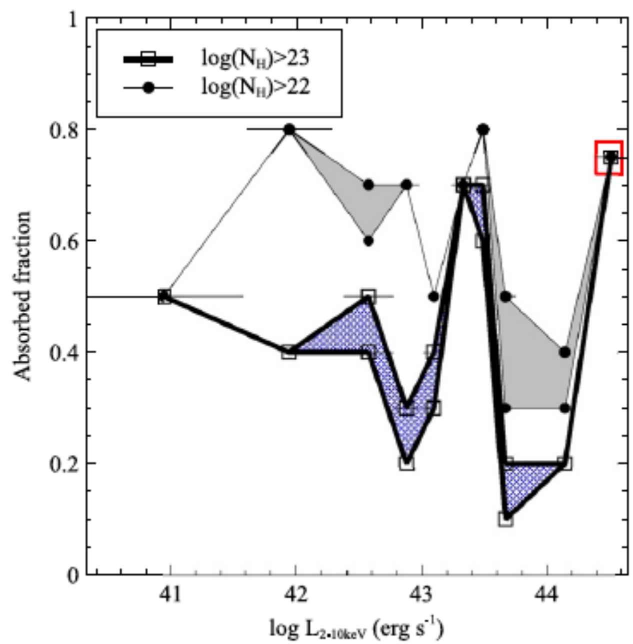

Figure 13. Absorbed fractions against intrinsic 2–10 keV luminosity (10 objects per bin). Filled circles connected by thin solid lines show the fraction of sources with $\log(N_{\rm H}) > 22$, whereas empty squares connected by thick lines show the fraction of sources with $\log(N_{\rm H}) > 23$. The solid gray and blue hatched shading reveal the uncertainty in these fractions due to the 13 sources with ambiguous spectral types (and hence two estimates for their $\log N_{\rm H}$). The absorbed fraction in the highest luminosity bin (indicated by the red square) is more uncertain since it contains only four objects.

Photon index vs. Luminosity

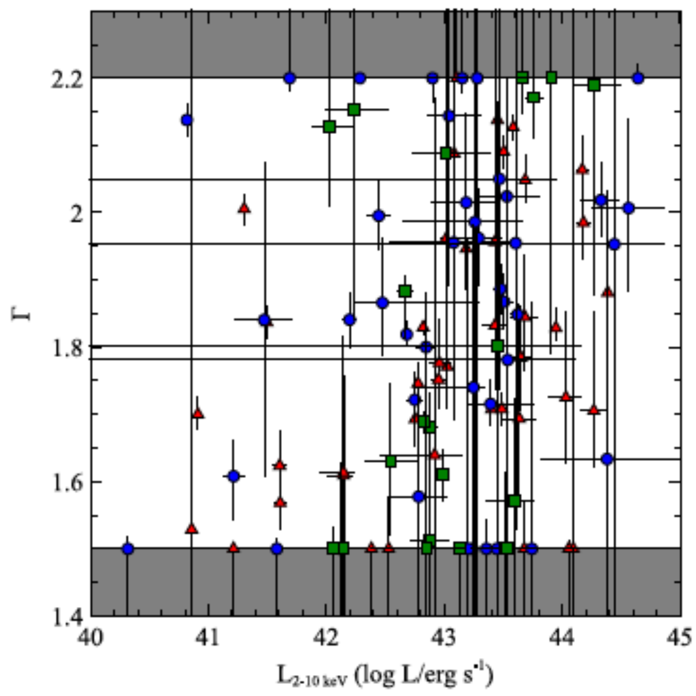

Figure 15. Photon index Γ against intrinsic (absorption-corrected) 2–10 keV luminosity $L_{2-10\,\mathrm{keV}}$. The gray shaded areas delineate the hard limits imposed on Γ in the fit.

Soft excess strength vs. photon index

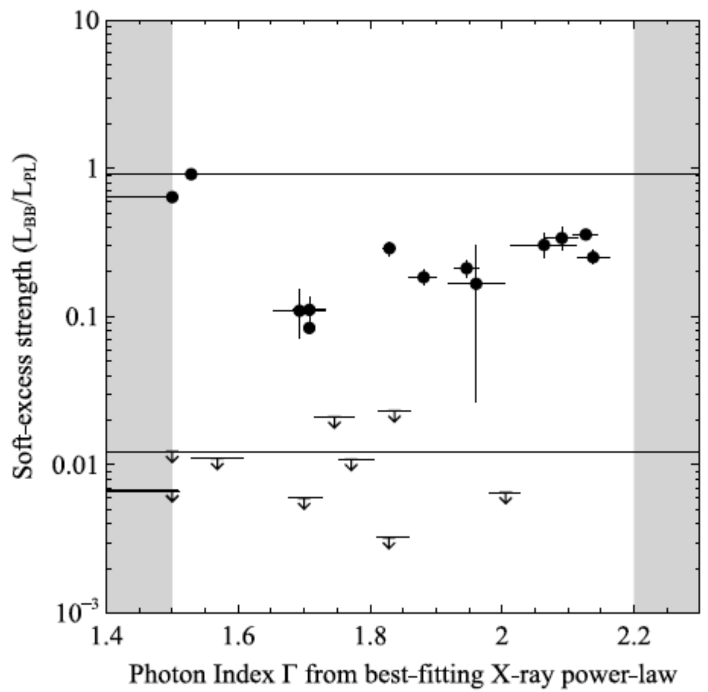

Figure 23. Soft-excess strength against photon index Γ. The soft-excess strength is parameterized as described in Figure 22. Downward-pointing arrows show upper-limiting soft-excess strengths wherever a source did not have a statistically significant soft excess (using the ZBBODY model).

Reflection properties (using BAT+XMM)

Table 5
Reflection Fit Results for Objects with *XMM-Newton* Data, Fit in Conjunction with BAT Data

AGN	Partial Covering? (1)	BAT Renormed? (2)	R (3)	$E_{\rm fold}$ (4)	$\Gamma_{\rm PEXRAV}$ (5)	$\Delta\Gamma$ (6)
3C 234	Y	Y	<0.58	138^{+1594}_{-85}	$2.03^{+0.14}_{-0.13}$	-0.17
NGC 3227	Y	...	$12.86^{+3.10}_{-3.14}$	>636	$2.08^{+0.05}_{-0.09}$	0.58
Mrk 417	Y	Y	<0.45	38^{+13}_{-17}	$0.75^{+0.08}_{-0.31}$	-1.31
Mrk 728	...	...	$0.07^{+3.10}_{-0.07}$	616_{-570}	$1.70^{+0.38}_{-0.09}$	-0.07
IC 2637	...	Y	$1.09^{+2.38}_{-0.91}$	>156	$1.79^{+0.24}_{-0.09}$	0.10

Reflection vs. luminosity for stacked spectra

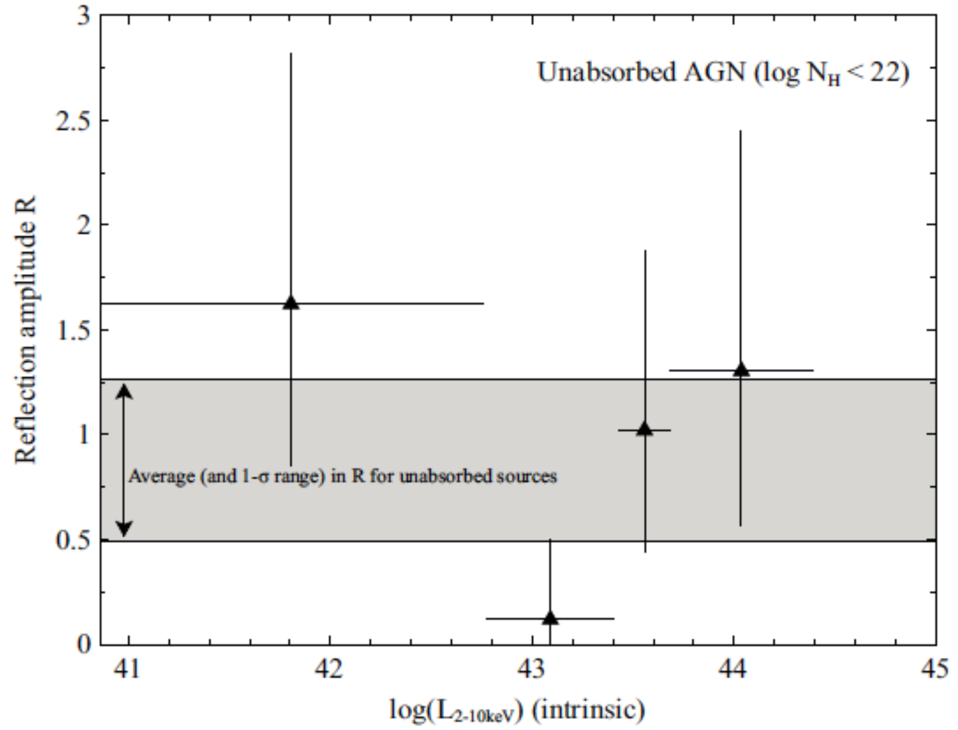

FIG. 4.— Reflection vs intrinsic 2–10 keV luminosity for log N_H < 22 sources, stacked in different luminosity bins.

Summed soft spectrum from entire catalogue

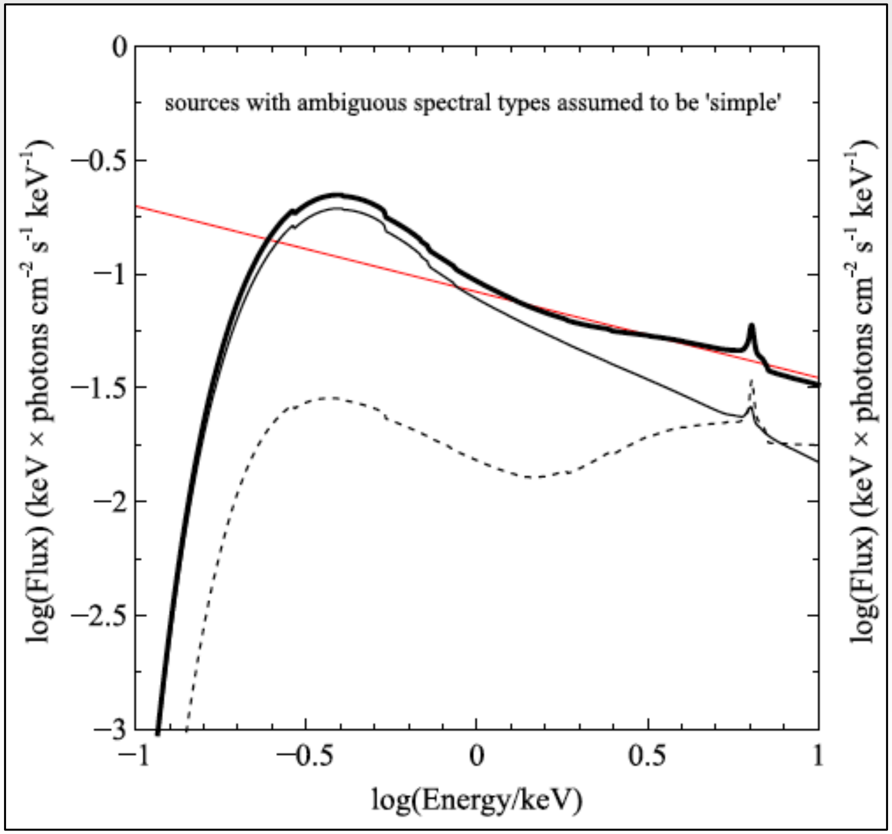

'Evolution' of the BAT AGN with flux limit

Table 6
Comparing BAT Catalogs: Flux Limits, Completeness, and Absorption Properties

Catalog (1)	Flux Limit (2)	Completeness Limit (3)	Ambiguous Sources (4)	$\log(N_H > 22)$ (5)	$\log(N_H > 23)$ (6)	$\log(N_H > 24.15)$ (C-thick) (7)	Simple Abs. ($\langle \log N_H \rangle, \sigma$) (8)	Complex Abs. ($\langle \log N_H \rangle, \sigma$) (9)
9 month	−10.70	−11.0	0%	55%	33%	0% (<6%)	45% (20.58,0.74)	55% (23.03,0.71)
22 month	−10.96	−11.25	10%	59%–64%	49%–54%	5% (<18%)	36%–46% (20.47–20.56, 0.86–0.90)	54–64% (23.28–23.4, 0.57–0.68)
58 month	−11.40	−11.6	13% †	57%–61%	41%–45%	9% (<15%)	38%–50% (20.67–20.80, 1.12–1.18)	43–56% (23.27–23.55,0.71–0.95)

Notes. (1) Catalog. (2) Logarithm of BAT flux limit (14–195 keV) in erg cm^{-2} s^{-1}. (3) Completeness limit, given as $\log(S)$ for 2–10 keV flux S in units of erg cm^{-2} s^{-1}. (4) Percentage of sources with ambiguous spectral types. (5) Percentage of sources with $\log(N_H) > 22$. (6) Percentage of sources with $\log(N_H) > 23$. (7) Percentage of Compton-thick sources, with $\log(N_H) > 24.15$ (upper limits are based on consideration of the other Compton-thickness metrics discussed in Section 5.1). (8) Percentage of simple absorption sources, with average column density and standard deviation. (9) Percentage of complex-absorption sources, with average column density and standard deviation. Ranges in these values are due to sources with ambiguous spectral types. † An additional 5% of our 58 month sources do not have enough counts to construct a spectrum, so these are not classified into any of the categories shown here.

Future work: multi-wavelength AGN SEDs for a complete sample

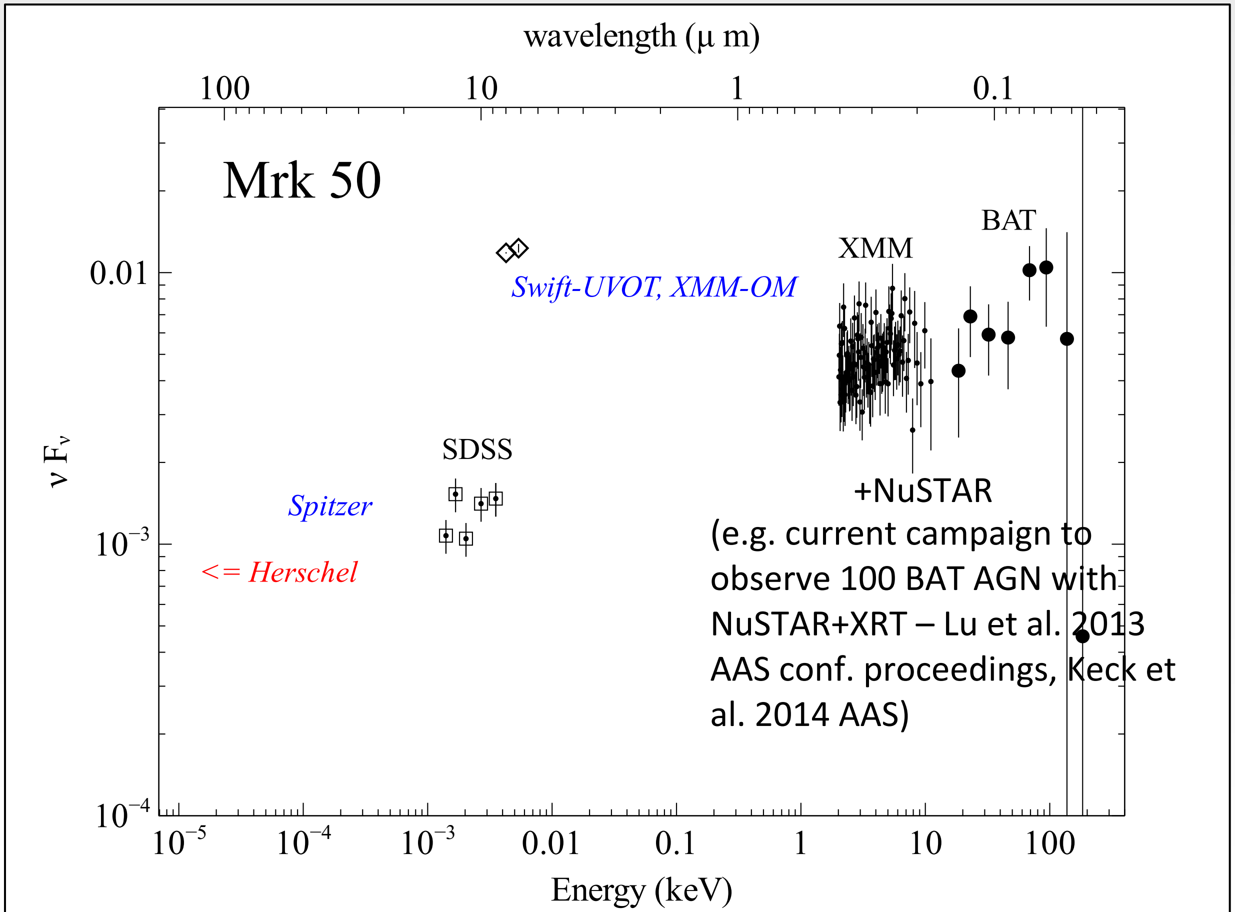

+NuSTAR

(e.g. current campaign to observe 100 BAT AGN with NuSTAR+XRT – Lu et al. 2013 AAS conf. proceedings, Keck et al. 2014 AAS)

log N – log S

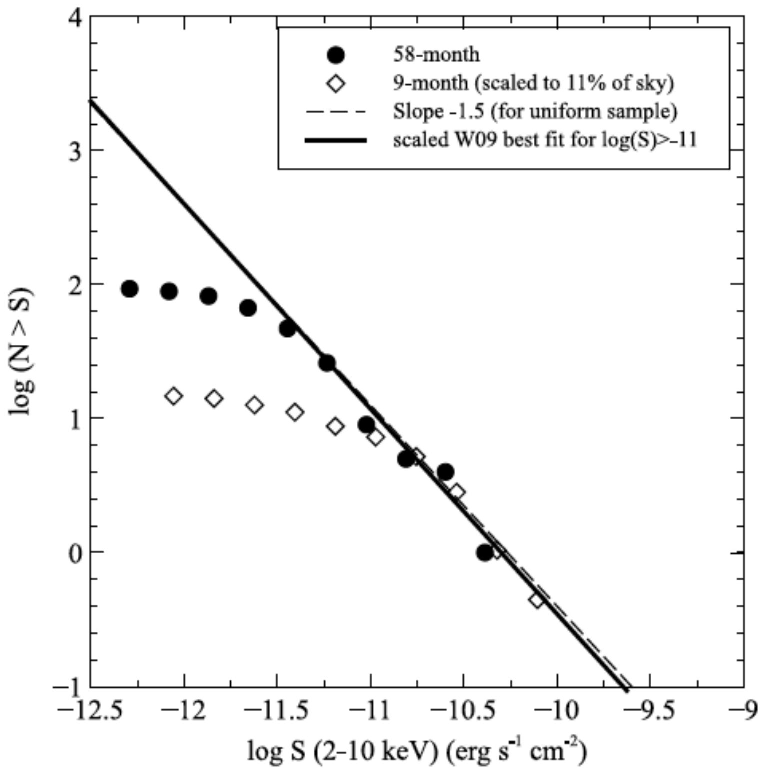

Figure 30. Plot of $\log(N > S)$ against $\log(S)$, for 2–10 keV flux S in $\mathrm{erg\,s^{-1}\,cm^{-2}}$, where $\log(N > S)$ is the logarithm of the number of sources with flux greater than S. The thin line shows a slope of -1.5 expected for a uniform distribution. Our sample shows a slope consistent with this down to fluxes of $\log(S) = -11.6$.